Vehicular Communications 24 (2020) 100246

Contents lists available at ScienceDirect

Vehicular Communications

www.elsevier.com/locate/vehcom

Harnessing retroreflective transportation infrastructure for intelligent vehicle positioning

Sihua Shao [a,*], Abdallah Khreishah [b]

[a] Department of Electrical Engineering, New Mexico Tech, Socorro, NM 87801, United States of America
[b] Department of Electrical and Computer Engineering, New Jersey Institute of Technology, Newark, NJ 07102, United States of America

ARTICLE INFO

Article history:
Received 29 September 2019
Received in revised form 9 January 2020
Accepted 8 February 2020
Available online 13 February 2020

Keywords:
Retroreflectivity
Intelligent transportation system
Vehicle positioning
Angle-of-arrival
Dead reckoning
Kalman filter

ABSTRACT

The popularity of intelligent transportation system (ITS) applications urges the development of vehicle positioning system that satisfies the availability, precision and accuracy requirements. Lane level (the exact lane on the road) positioning or even in-lane level (the exact location within the lane) positioning are expected in all driving environments at all times. In addition to the existing vehicle positioning technologies, such as Global Positioning System (GPS), terrestrial radio (e.g., cell phone, AM, FM and digital TV) and feature-based sensors (e.g., vision, LiDAR and RADAR), we propose a complementary vehicle positioning system based on ubiquitous retroreflective transportation infrastructures. Low-cost photodiodes are mounted on the headlights to sense the retroreflected optical signals from on-road safety device, such as raised pavement marker (RPM). A liquid crystal display (LCD) shutter is installed on the RPM to distinguish the retroreflected light signals from different RPMs and from the environmental reflection. By sensing the angle-of-arrival of the retroreflected light beam from the RPMs (i.e., landmarks), the vehicle realizes lane level positioning based on triangulation. Advanced positioning solution is proposed by integrating dead reckoning and Kalman filter to advance the lane level positioning to in-lane level positioning. Extensive experimental results reveal that the proposed vehicle positioning system achieves sub-meter level location accuracy.

1. Introduction

The advancement of intelligent transportation system (ITS) applications, such as lane change warning, optimal lane selection, or even autonomous driving, requires more precise position information than that provided by low-cost Global Positioning System (GPS). Although the current in-vehicle navigation systems provide the drivers with reliable guidance to travel from one location to another in the simple form of a line and the traveling direction, they lack the details related to lane level positioning (which lane on the road) and even in-lane level positioning (where in the lane). Combining the lane level information with the communication among connected vehicles, the real-time optimal traveling lane can be determined even in dense traffic. Also, the appropriate line for exiting can be selected earlier which minimizes the risk of the last-second lane changes, especially in busy expressways.

GPS [1–4], terrestrial radio [5–7] and feature-based sensors [8,9] have been investigated in many earlier works to pursue a low-cost, robust, highly-accurate and highly-available vehicle positioning system. However, GPS and terrestrial radio approaches either endure high location error especially in urban areas or require expensive additional infrastructure deployments. Feature-based sensors achieve high location accuracy with the constraints of high power consumption, high processing latency and limited range. In addition to all of the existing approaches, we propose a low-cost, low-delay, highly-accurate and highly-secure vehicle positioning system by utilizing the ubiquitous retroreflective transportation infrastructures as landmarks (Fig. 1).

Recent progress on retroreflecter-based visible light communication (VLC) [10,11] elucidates the great potential of applying retroreflective on-road safety devices to intelligent vehicle positioning system. Different from mirror reflection, retroreflection reflects the light back to its source with minimal scattering, which ensures the alignment between the light source and the retroreflector. The proposed system works similarly to an RFID system. In particular, the reader (i.e., a transceiver) is a VLC enabled illuminating device equipped with the photosensor (e.g., photodiode) as the receiver. A micro control unit (MCU)-controlled liquid crystal

* Corresponding author.
E-mail addresses: sihua.shao@nmt.edu (S. Shao), abdallah@njit.edu (A. Khreishah).

https://doi.org/10.1016/j.vehcom.2020.100246
2214-2096/

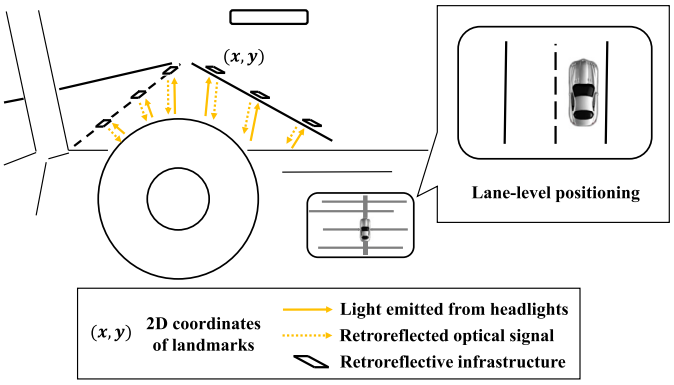

Fig. 1. Lane level positioning based on retroreflective transportation infrastructures.

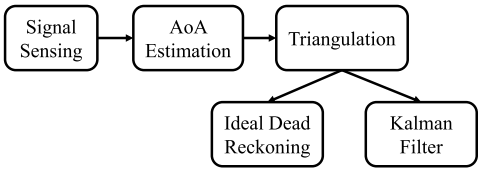

Fig. 2. Block diagram for the proposed positioning method.

display (LCD) shutter and a retroreflective device (e.g., corner-cube, sheet, spray, etc) constitute the tag, which receives the downlink information from the reader and piggybacks the dynamic information of interest (e.g., coordinates and identification) on the uplink through modulating the reflected light beam with the LCD shutter atop the retroreflective surface. The LCD shutters also allow the retroreflected optical signals to be distinguished from the reflection of other on-road objects and from different RPMs. The proposed positioning system consists of two readers and multiple tags. The two readers are the left and the right headlights equipped with photodiodes on each headlight as the receiver. The tags are constituted by the on-road safety devices (e.g., raised pavement markers (RPMs), traffic signs and license plates, etc.) and the MCU-controlled LCD shutters. Therefore, the vehicles, the infrastructure, the policemen and the roadways are already equipped with the basic devices needed in the intelligent vehicle positioning system. In addition to vehicle positioning, the proposed system can also be utilized to enable other ITS applications (Sec. 3). In this paper, we focus on the discussion about utilizing the proposed system for vehicle positioning.

As shown in Fig. 2, upon sensing the retroreflected optical signals from the RPMs, the proposed positioning system performs angle-of-arrival (AoA) estimation (Sec. 4.1) to extract the incidence angle of the retroreflected light beam. Based on the estimated AoAs, triangulation based positioning approach is adopted (Sec. 4.2) to achieve lane level positioning. To further enhance the location accuracy, two approaches - ideal dead reckoning (Sec. 5.2) and Kalman filter (Sec. 5.3) are integrated individually by taking into account the traveled distance from a reference location to realize in-lane level positioning. Extensive experimental results (Sec. 7) indicate sub-meter level location error.

The proposed vehicle positioning system enjoys many superior features. In addition to the low deployment cost [10], the system operates in a directed and reactive manner, which minimizes the eavesdropping range of man-in-the-middle or jamming attacks. Also the system receives information in line rate by avoiding any delay incurred by image processing. The capability of dynamic information delivering from the tags to the readers makes the joint vehicle positioning and infrastructure-to-vehicle (I2V) communication pervasively available.

Our major contributions are summarized as follows:

- We propose a new lane level vehicle positioning approach by utilizing ubiquitous retroreflective transportation infrastructures, such as raised pavement markers, as landmarks.
- Based on the observation of the distribution of location error, we advance the lane level positioning to the in-lane level positioning by integrating dead reckoning and Kalman filter.
- We experimentally evaluate the 2D location accuracy, horizontal and vertical location errors, and the average trajectory of the lane level and the in-lane level positioning methods. The results reveal that the location error of lane level positioning method is dominant in vertical direction and in-lane level positioning method achieves sub-meter level location accuracy with median location error at 0.2 meters.

2. Related work

Global positioning system Based on satellites continuously transmitting data about their current time and position, the Global Positioning System (GPS) receiver determines its location according to its own synchronized clock [1]. The location error of a traditional GPS-enabled smartphone is typically 4.9 meters [12]. When using GPS receivers in street canyons with tall buildings, the shadowing and multipath effects may contribute to poor GPS signal reception [3]. Differential Global Positioning System (DGPS) [4] enhances the location accuracy of traditional GPS to centimeter level in case of the best implementations by utilizing fixed ground-based reference stations to broadcast the difference between the positions indicated by the GPS satellite system and known fixed positions. The DGPS receivers, which receive the difference from the ground-based reference stations, correct their positions by the same amount. DGPS relies on additional deployment of reference stations that are not commonly available. Exclusively relying on GPS is inadequate to meet the requirements of the emerging ITS applications due to the blockage of obstacles. Our proposed system enables accurate vehicle positioning pervasively to support lane level or even in-lane level positioning in the situations where GPS signal is insufficient.

Terrestrial radio Pseudolites [5], contraction of “Pseudo-Satellite”, are small transceivers deployed on the ground to perform the similar functions of GPS. As ground-based GPS alternatives, Pseudolites work as complementary local positioning system for the places where the GPS signals are blocked, jammed or simply not available. Such radio-based local positioning system still suffers the blockage and multipath problems like GPS, especially in urban canyon. Cell phone localization [6] is an alternative method to supplement the in-car navigation system. Based on measuring the received signals from the closest base stations, the cell phone estimates the distances between itself and the nearby base stations. Received signal power, time of arrival and time difference of arrival are typical approaches to evaluate the distances. Multilateration or triangulation is utilized to determine the location of the cell phone. The location accuracy of cell phone localization is generally less than that of GPS. In urban areas where the density of base stations is sufficiently high, the cell phone determines its location more precisely than in rural areas. AM, FM and digital TV radio signals have better received power levels than that of GPS in urban areas and are capable of penetrating through buildings. However, the location accuracy [7] is still at meter level which is inadequate to support lane level positioning. According to the experimental results (Sec. 7), our proposed system achieves sub-meter level location accuracy by relying on the ubiquitously deployed on-road safety devices.

Feature-based sensors LiDAR [8] as an emerged 3D scanning technology, measures the distance to an object by sending pulsed laser

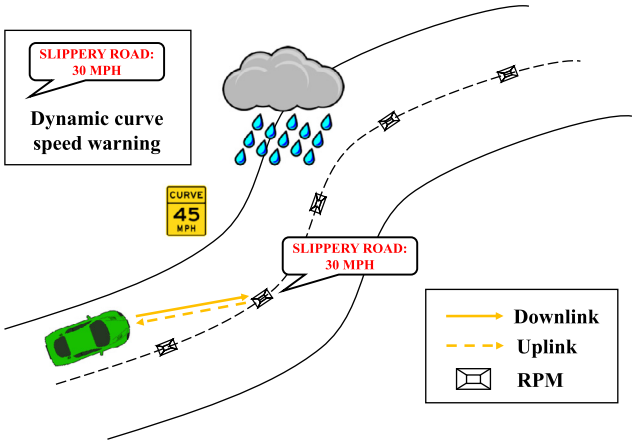

Fig. 3. Curve speed warning.

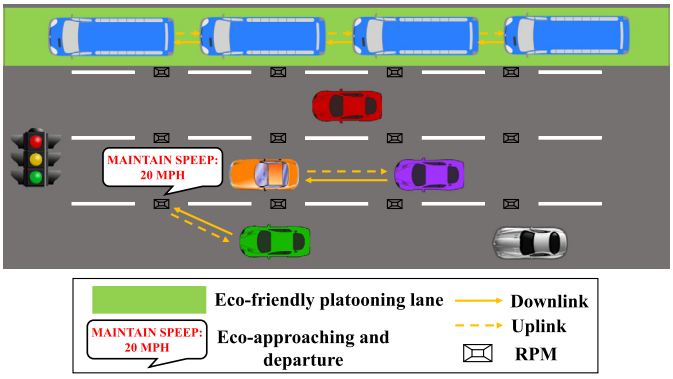

Fig. 4. Platooning and speed advising.

and sensing the reflected pulses. LiDAR provides full 360 degree environmental view for use in autonomous vehicles. However, LiDAR is only capable of sensing the profiles of the targets rather than generating a colorful image like camera does, which indicates that LiDAR can only detect the lateral distance to the curb rather than the lateral offset from the central line of a lane. In addition to the high expense issue of LiDAR devices, one potential problem is that the physically spinning mirror has to endure the bumps and acceleration of everyday driving. Another fact that one cannot entirely discount is that the physical form of the LiDAR unavoidably affects the beautiful appearance of the car. Camera-based vehicle sensing technology [9] is similar to LiDAR, taking into account the difference in terms of sensing capability. Even though camera is able to capture more information (e.g., color) than LiDAR, such as the dash and solid lines between the lanes, the image processing latency [9] and the limited range cause problems in delay sensitive applications such as emergency brake warning. Our proposed system reuses the existing transportation infrastructures which reduces the deployment cost and also incurs much less latency than image processing.

Infrastructural support Some earlier literature also considered utilizing the on-road infrastructures to pave the way for intelligent transportation systems. In [13], a wireless sensor package has been developed to instrument roadways. The sensor package counts passing vehicles, measures the average speed of the vehicles, and detects weather conditions such as ice and water on the road. Information collected by the clusters of sensors can be forwarded in near real-time to wired base stations. The control unit can utilize the information for use controlling, predicting traffic, and clearing road hazards. [14] reuses the already-installed cat's eyes which are placed along the road on both sides of a highway and simply replaces the existing nodes with the smart nodes. Sensors are placed inside the cat's eyes to form a network. In the network, each node can disseminate the information (e.g., occurrence and location at a particular timing) about each vehicle to the other nodes.

3. Use cases

The proposed system that utilizes retroreflective on-road safety devices can assist in different applications of ITS related to safety, energy-saving, and positioning. Here we discuss some typical application scenarios.

Curve speed warning based on real-time road surface conditions Vehicles entering the curves with excessive speed may lead to lane departure, collision or loss of vehicle control, which may result in injury or death. Static curve speeding warning only considers the road geometry and may advise insufficient reduced speed limit. Taking into account the real-time road surface conditions, the drivers need to be notified in advanced of a curve if the speed is above the safe limit. In Fig. 3, although the road sign has a speed limit of 45 mph based on the curve geometry, in a rainy day, the wet road surface may have lower sliding coefficients of friction, which indicates that the safe speed limit should be lower than 30 mph. The vehicle negotiates with RPMs (i.e., also the landmarks when they are utilized for vehicle positioning) in advance of the curve to determine the appropriate speed based on road surface parameter. The application of curve speed warning has the potential to jointly perform speed detection and speed warning in a real-time manner along the traveling path.

Energy-saving and eco-friendly applications In Fig. 4, by connecting the vehicles driving in the same lane through the retroreflective connectivity between the headlight and the license plate, the concept of platooning can be realized. The distance estimation between vehicles enabled by platooning also assists in the vehicle positioning in the global frame of reference. Grouping vehicles in to platoon reduces the times of stop-and-go and consequently minimizes the fuel consumption and the greenhouse gas emission. Compared to RF-based approaches, security vulnerabilities under various attacks from adversaries is alleviated by exploiting the directivity and impermeability of light. Also taking advantage of the knowledge about the timing of traffic signals, the dynamic information piggybacked by the landmarks (i.e., RPMs) are able to advise the optimal speed of the vehicles in order to make fewer stops.

4. From AoA sensing to lane level positioning

AoA and triangulation based positioning methods have been studied both in RF systems [15] and line-of-sight (LOS) based VLC systems [16,17]. However, sensing the AoA of a retroreflective link requires additional analysis of the channel characteristics. In this section, we apply the PD-based AoA sensing technique [17] to a retrorefletive link and discuss the adoption of AoA sensing in our proposed vehicle positioning system.

4.1. AoA sensing principles

Pulsar [17] proposes a sparse photogrammetry approach by utilizing a "single-pixel" PDs to circumvent the limitations of the camera-based traditional photogrammetry such as limited range, high processing latency and high power consumption. The main idea is to use two physically co-located PDs with different field-of-views (FOVs) to form the receiver. The ratio of two received signals strength (RSSs) can be uniquely mapped to the incidence

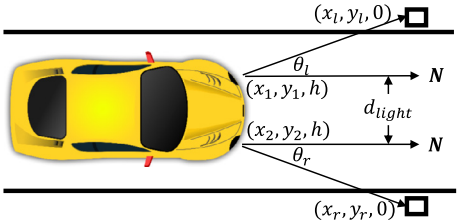

Fig. 5. AoA-based positioning utilizes two RPMs as landmarks.

angle of the light beam from an approximated point light source. The reason behind the unique mapping is that the two links have the same transmitter and channel gains while the only difference is the receiver gain. Assume we have two PDs with different FOVs placed on one of the vehicle's headlights, the RSSs of both PDs from one RPM can be represented by

$$RSS_1 = P_t A_t(\theta_1)\alpha(2r_1)R(\theta_1)A_{r1}(\theta_1)$$
$$RSS_2 = P_t A_t(\theta_2)\alpha(2r_2)R(\theta_2)A_{r2}(\theta_2)$$

where P_t is the amount of the emitted optical power that can be retroreflected back to the PD, $A_t(\theta)$ is the irradiance angular response at irradiance angle θ, $\alpha(2r)$ is the propagation loss at distance r since the light propagates from the headlight to the RPM and then back to the PD on the headlight, $R(\theta)$ is the attenuation caused by the retroreflection, and $A_{ri}(\theta)$ is the incidence angular response of the i-th PD at incidence angle θ. Note that due to retroreflectivity, the value of the irradiance angle is the same as that of the incidence angle. Since the two PDs are physically co-located with negligible separation compared with r, we can safely assume $\theta_1 = \theta_2 = \theta$ and $r_1 = r_2$. Dividing RSS_1 by RSS_2, all other factors related to the characteristics of the light, distance and retroreflector will cancel out:

$$\frac{RSS_1}{RSS_2} = \frac{A_{r1}(\theta)}{A_{r2}(\theta)} = A_c(\theta).$$

Therefore, the AoA can be determined by a non-linear function A_c^{-1} which maps the ratio of RSSs to the incidence angle through

$$\theta = A_c^{-1}(\frac{RSS_1}{RSS_2}).$$

The non-linear function A_c^{-1} needs to be derived from the one-time factory calibration of PDs' angular response $A_{ri}(\theta)$. The unique mapping between the incidence angle and the ratio of RSSs relies on two approximations which are both valid under our positioning system settings. First, the function A_c^{-1} needs to be monotonic within the range of AoA. According to our experimental results (Fig. 11), the monotonic relationship between the AoA and the ratio is validated. Second, the light source can be approximated as a point source from the PDs' perspective. In our proposed positioning system, the light source from the PDs perspective is the RPM, of which the size is much smaller than the distance r. Therefore, the RPM can be approximated as a point light source.

4.2. AoA-based positioning

To move from AoA sensing to 2D positioning, two incidence angles and the distance between the headlights are taken into account to form a system of equations, which is resolved by the widely-used Levenberg-Marquardt algorithm [18]. As shown in Fig. 5, the AoA-based positioning utilizes two RPMs as landmarks, with one RPM at the left side and one RPM at the right side. Denote the locations of the left and the right headlights as $L_l = (x_1, y_1, h)$ and $L_r = (x_2, y_2, h)$, respectively, where h is the known vertical distance to the ground. The midpoint of the left and the right headlights $(\frac{x_1+x_2}{2}, \frac{y_1+y_2}{2}, h)$ represents the location of the vehicle. The two RPMs' locations $L = (x_l, y_l, 0)$ and $R = (x_r, y_r, 0)$ are known from decoding the retroreflected optical signals. Further, denote the unit normal vector of PDs' sensing surface as $\boldsymbol{N} = (a, b, c)$, which can be measured by motion sensors (compass, gyroscope, and accelerometer) installed on the vehicle. The line vector from the left headlight to the left RPM $\boldsymbol{V_{left}} = (x_l - x_1, y_l - y_1, -h)$ and the line vector from the right headlight to the right RPM $\boldsymbol{V_{right}} = (x_r - x_2, y_r - y_2, -h)$ are parallel to the incident light beams from the left and right retroreflective RPMs, respectively. Denote the AoAs of the left and the right beams by θ_l and θ_r, respectively, then we have

$$\cos\theta_l = \frac{\boldsymbol{N}\cdot\boldsymbol{V_{left}}}{|\boldsymbol{N}||\boldsymbol{V_{left}}|} \tag{1}$$

$$\cos\theta_r = \frac{\boldsymbol{N}\cdot\boldsymbol{V_{right}}}{|\boldsymbol{N}||\boldsymbol{V_{right}}|}. \tag{2}$$

Since the distance d_{light} between the left headlight and the right headlight is known, we also have

$$d_{light} = \sqrt{(x_1 - x_2)^2 + (y_1 - y_2)^2}. \tag{3}$$

To resolve the four unknowns (x_1, y_1, x_2, y_2) representing the vehicle's location, we only need AoA measurements from two RPMs to form a system of equations since (3) restricts the solutions to be inside the feasible region. When the retroreflected optical signals from the left and the right RPMs are sensed, we turn the equation solving into an optimization problem which minimizes the square errors between the summations of the left and the right hand sides of (1), (2) and (3),

$$\vec{s}_{opt} = \arg\min_{s} \sum f(\vec{s})^2,$$

where $\vec{s} = (x_1, y_1, x_2, y_2)$ and

$$f(\vec{s}) = (\cos\theta_l + \cos\theta_r + d_{light}) - (\frac{\boldsymbol{N}\cdot\boldsymbol{V_{left}}}{|\boldsymbol{N}||\boldsymbol{V_{left}}|} + \frac{\boldsymbol{N}\cdot\boldsymbol{V_{right}}}{|\boldsymbol{N}||\boldsymbol{V_{right}}|} + \sqrt{(x_1 - x_2)^2 + (y_1 - y_2)^2}).$$

To accelerate the search process for the above non-linear least square optimization problem, the widely-used Levenberg-Marquardt algorithm [18] is adopted.

It can be expected that as the vehicle moves towards the pair of RPMs, the location accuracy is getting higher. This is not only because the retroreflected optical signal strength increases, but also because the variation of the AoA increases with a certain traveled distance. For instance, assume a vehicle is traveling on the central line of a lane and denote the vertical distance between the vehicle and the pair of RPMs as d_v, the AoA variation when the vehicle moves from $d_v = 20\ m$ to $d_v = 18\ m$ is less than that when the vehicle moves from $d_v = 12\ m$ to $d_v = 10\ m$. In other words, the distinguishability of landmarks increases as the vehicle moves towards the pair of RPMs. However, if the vehicle is too close to the pair of RPMs, the retroreflected optical signal will disappear since the light emitted by the headlights no longer covers the pair of RPMs. Therefore, the location accuracy is at its peak when the vehicle is at the closest position to the pair of RPMs before the illuminated area of the headlights goes beyond the pair of RPMs. Once the vehicle crosses the current pair of RPMs, the vehicle positioning starts relying on the next pair of RPMs, which are generally far away from the vehicle and thereby the location accuracy drops

to the lowest level. As the vehicle moves towards the next pair of RPMs, the location accuracy keeps increasing until the vehicle crosses the next pair of RPMs. The analysis is validated by experimental results presented in Sec. 7.1. One interesting observation based on the experimental results (Fig. 12) is that even though the location error reaches up to several meters when the vehicle is far away from the pair of RPMs, the location error mainly occurs at the vertical direction (i.e., traveling direction) while the location error at the horizontal direction (i.e., the offset from the central line of the lane) is less than one meter. The observation reveals two facts: 1) relying only on the triangulation method is sufficient to support lane level positioning; 2) the location error can be significantly reduced by integrating dead reckoning, which exploits mobility to enhance positioning accuracy [19]. The principles of dead reckoning and the advanced positioning solution are demonstrated in the next section.

5. Dead reckoning based in-lane level positioning

5.1. Dead reckoning principles

Dead reckoning [19] is the process of tracking the current location of a moving object based on a previously determined location (i.e., typically determined by fixed landmarks), the moving speed, the moving direction and the elapsed time. Dead reckoning can always provide available information on location. However, it suffers from cumulative errors since the actual speed and direction cannot be measured perfectly at all time instants. For example, in automobile navigation, if the traveled distance between two time instants is estimated by the number of rotation of the wheels, any divergence between the actual and the estimated traveled distance per rotation, caused by the slippery or irregular road surfaces, turns into a source of error. Therefore, dead reckoning is typically integrated with accurate but occasionally unavailable positioning methods to generate a combined position fix.

5.2. Advanced positioning solution

In our proposed lane level positioning system (Sec. 4.2), as the vehicle travels across each pair of RPMs, the accurate location information can be obtained through the AoA and triangulation based positioning periodically. To determine the location of the vehicle between two pairs of RPMs, the traveled distance since the last recorded location is integrated into the system of equations elaborated in Sec. 4.2. As shown in Fig. 6, a vehicle is traveling from left to right. At location (x_c, y_c), the vehicle calculates its location accurately based on the measurements of the retroreflected optical signals from RPMs 1 and 2. When the vehicle moves to the location (x_n, y_n), the vehicle cannot receive the optical signals retroreflected from RPMs 1 and 2 and thereby relies on the optical signals retroreflected from RPMs 3 and 4. However, since the vehicle is still far away from RPMs 3 and 4, the received signal strength is weak such that the estimated location is inaccurate. Note that at location (x_c, y_c), even though the vehicle can detect the signals from RPMs 3 and 4, the vehicle only utilizes the measurements of the signals from RPMs 1 and 2 to perform positioning since the measurements of weak signals from additional landmarks will only degrade the location accuracy. One intuitive solution may be reducing the interval between RPMs (i.e., distance between RPMs 1 and 3 or RPMs 2 and 4). However, reducing the RPM interval will essentially increase the deployment cost and also violate the regulations [20]. Therefore, we utilize the distance

$$D = \sqrt{(x_n - x_c)^2 + (y_n - y_c)^2} \tag{4}$$

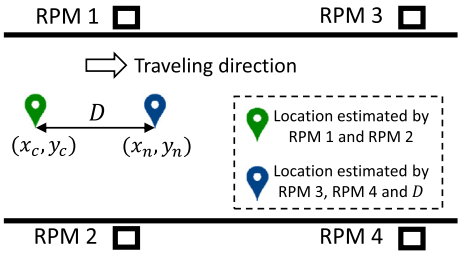

Fig. 6. Advanced positioning integrates dead reckoning.

to enhance the location accuracy at location (x_n, y_n). D can be estimated by the sensors equipped on vehicles for anti-lock braking system and electronic stability control. Ideally, for each pair of RPMs (e.g., RPMs 1 and 2 in Fig. 6, if the accurate location information (x_c, y_c) can always be successfully tracked by detecting the variation of retroreflected optical signal strength, due to the short interval of RPMs, the cumulative error of the estimated D is generally negligible [21]. Therefore, the location of the vehicle can be determined by minimizing the square errors between the summations of the left and the right hand sides of (1), (2), (3) and (4),

$$\overrightarrow{s}_{opt} = \arg\min_{s} \sum f(\overrightarrow{s})^2,$$

where $\overrightarrow{s} = (x_1, y_1, x_2, y_2)$,

$$x_n = \frac{x_1 + x_2}{2}, \quad y_n = \frac{y_1 + y_2}{2}$$

and

$$f(\overrightarrow{s}) = (\cos\theta_l + \cos\theta_r + d_{light} + D) - \left(\frac{\boldsymbol{N} \cdot \boldsymbol{V_{left}}}{|\boldsymbol{N}||\boldsymbol{V_{left}}|} + \frac{\boldsymbol{N} \cdot \boldsymbol{V_{right}}}{|\boldsymbol{N}||\boldsymbol{V_{right}}|} + \sqrt{(x_1 - x_2)^2 + (y_1 - y_2)^2} + \sqrt{(x_n - x_c)^2 + (y_n - y_c)^2}\right).$$

However, if the detection of one pair of RPMs is failed due to bumping, the vehicle will lose the track of its current location. To resolve this problem, Kalman filter is integrated with the dead reckoning approach in the next subsection.

Kalman filter [22,23] has been widely used for vehicle navigation by the fusion of noisy measurement and sensor-based prediction. The work in [22] integrates the vehicle sensors, such as wheel speed sensors, steering angle encoder and a fiber optic gyro with an extended Kalman filter for the purpose of achieving enough accuracy to enable in-vehicle cooperative collision warning. Adaptive algorithms with a conventional Kalman filter for vehicle navigation are proposed in [23] to accommodate sudden changes of vehicle motion and measurement errors. To circumvent the requirement of successfully detecting each pair of RPMs at the highest retroreflected optical signal strength, we propose to combine Kalman filter with the dead reckoning estimation such that only the accurate initial location of the vehicle is needed.

Instead of ideally assuming the estimation error of D to be negligible, we consider more practical conditions where the estimation error of D consists of some uncertain external influence such as slipped wheel, wind effect and bumpy road. As the variation of D is roughly linear in a short-term, we use a discrete-time linear system to approximate the evolution of the value of D over time. A first-order Kalman filter is adopted to update the measurement of D (i.e., the distance between the current location estimated by AoA-based positioning and the initial reference location) by the prediction based on vehicle speed sensor.

We first establish the dynamic system model for the variation process of the value of D. We discretize the time into different

equal-length time slots which are the intervals between consequent location estimations at time t and time $t+1$. Denote D_t as the state at time t, the corresponding dynamic model can be represented by

$$D_{t+1} = FD_t + B(v_t + w_t) \tag{5}$$

where F is the state transition matrix and B is the control matrix applied to the discrete process D_t. The external uncertainty is modeled as w_t which is the Gaussian distributed noise with covariance Q and $Q = E[w_t w_t^T] = \sigma_w^2$. In our proposed model, we assume that the vehicle speed v_t (i.e., the first order derivative of the variation of D_t) is stable between t and $t+1$. Therefore, based on basic kinematic formula, we have $F = 1$ and $B = \triangle t$. To refine the prediction in (5) with measurements, the measurement equation is defined as

$$z_t = HD_t + n_t \tag{6}$$

where z_t denotes the observation variable, i.e., the traveled distance D_t computed based on the result of AoA-based positioning. H is the scale matrix for mapping the unit and scale of the state we are keeping track of to those of the readings. Since z_t is the direct observation of D_t, we have $H = 1$. n_t is the Gaussian distributed measurement noise with covariance R and $R = E[n_t n_t^T] = \sigma_n^2$.

5.3. Advanced positioning solution with Kalman filter

In each time slot, Kalman filter runs two estimations simultaneously. The priori estimation $D_{t+1|t}$ (in (5)) is performed to predict the state in the next time slot. The posteriori estimation $D_{t|t}$ is performed by combining both the observed measurement z_t (in (6)) and the priori estimation at the previous time slot $D_{t|t-1}$. Without loss of generality, the covariances of $D_{t+1|t}$ and $D_{t|t}$ are represented by $P_{t+1|t}$ and $P_{t|t}$, respectively.

Kalman filter has two phases in each time slot: updating and predicting. In the predicting phase, the priori estimation $D_{t|t-1}$ and $P_{t|t-1}$ are calculated based on the posteriori estimation $D_{t-1|t-1}$ and $P_{t-1|t-1}$. In particular,

$$D_{t|t-1} = FD_{t-1|t-1} + Bv_t,$$
$$P_{t|t-1} = FP_{t-1|t-1}F^T + Q.$$

In the updating phase, the posteriori estimation $D_{t|t}$ and $P_{t|t}$ are calculated based on the priori estimation $D_{t|t-1}$, $P_{t|t-1}$ and the observed measurement z_t. In particular,

$$D_{t|t} = D_{t|t-1} + K_t(z_t - HD_{t|t-1}), \tag{7}$$
$$P_{t|t} = P_{t|t-1} - P_{t|t-1}K_tH,$$

where K_t is the Kalman gain and defined by

$$K_t = P_{t|t-1}H^T(HP_{t|t-1}H^T + R)^{-1}. \tag{8}$$

The update equation (7) indicates that the Kalman gain K_t determines the dependency of the posteriori estimation $D_{t|t}$ on the observed measurement z_t and the prediction derived from $D_{t|t-1}$. If the measurement noise is low, which means that the value of R is small, based on (7) and (8), $D_{t|t}$ depends mostly on z_t. In contrast, if the external uncertainty imposed on the prediction in (5) is small, which means that the value of Q is small, based on (7) and (8), $D_{t|t}$ ignores z_t and relies instead on the prediction derived from $D_{t|t-1}$. In the experiments (Sec. 7), we empirically set both Q and R to 1 to balance the dependency.

The advanced positioning solution with Kalman filter is summarized in Fig. 7. The inputs of the Kalman filter are the vehicle speed

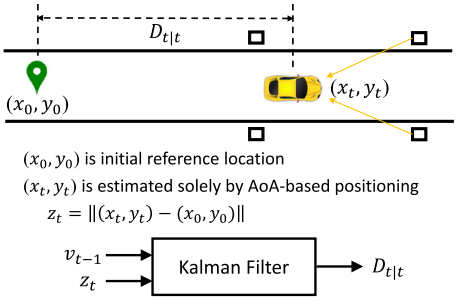

Fig. 7. Advanced positioning solution with Kalman filter.

v_{t-1} and observed measurement z_t. The output is the updated traveled distance $D_{t|t}$ since the initial reference location (x_0, y_0). The updated $D_{t|t}$ is then substituted into

$$D_{t|t} = \sqrt{(x_t - x_0)^2 + (y_t - y_0)^2}. \tag{9}$$

The location of the vehicle can be determined by minimizing the summation of the differences between the left side and the right side of (1), (2), (3) and (9),

$$\overrightarrow{s}_{opt} = \arg\min_{s} \sum f(\overrightarrow{s})^2,$$

where $\overrightarrow{s} = (x_1, y_1, x_2, y_2)$,

$$x_t = \frac{x_1 + x_2}{2},\ y_t = \frac{y_1 + y_2}{2}$$

and

$$f(\overrightarrow{s}) = (\cos\theta_l + \cos\theta_r + d_{light} + D_{t|t}) - \left(\frac{\boldsymbol{N}\cdot\boldsymbol{V_{left}}}{|\boldsymbol{N}||\boldsymbol{V_{left}}|} + \frac{\boldsymbol{N}\cdot\boldsymbol{V_{right}}}{|\boldsymbol{N}||\boldsymbol{V_{right}}|} + \sqrt{(x_1 - x_2)^2 + (y_1 - y_2)^2} + \sqrt{(x_t - x_0)^2 + (y_t - y_0)^2}\right).$$

6. Experimental setup

To evaluate the location accuracy of the AoA and triangulation based positioning method (Sec. 4) and the advanced positioning solution (Sec. 5), we conduct experiments to measure the RSS at different vertical distances. The measurements are performed 100 times at each vertical distance. As shown in Fig. 8, the testbed consists of a vehicle (Honda Civic 2009), two co-located PDs (BPV10 and BPW34) placed above the headlights, a raised pavement marker covered by an LCD shutter, and the oscilloscope (Tektronix MDO4034-3) for recording the time-domain data samples. Each PD working in photoconductive mode to measure the light intensity is driven by a 10 V DC and cascaded with a 6.8kΩ resistor. The RSS of each PD is linearly proportional to the output voltage of the resistor, which is measured by the oscilloscope. The recorded time-domain data samples are processed in MATLAB through Fast Fourier Transform (FFT) to compute the signal amplitude at a certain frequency, which is the modulation frequency of the LCD shutter. The diagram of the measurement setup is shown in Fig. 9. To evaluate the variation of the RSSs of the two PDs when the vehicle is moving towards the RPMs, we change the position of the RPM instead of moving the vehicle. The RPM equipped with the LCD shutter is placed along the lines which are 60 cm away from the left and the right headlights, respectively. The intervals of the candidate positions of the RPM are all set to 1 m. Thanks to the retroreflectivity of the RPMs, the light from the left and the right

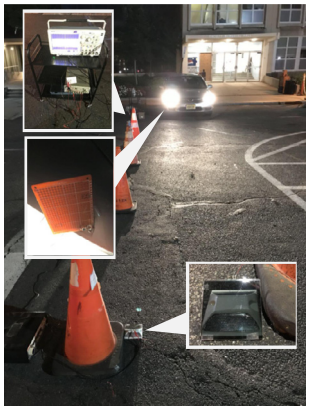

Fig. 8. Testbed.

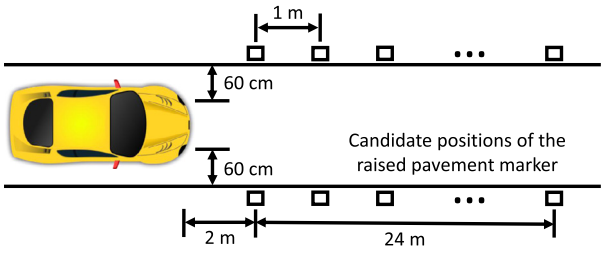

Fig. 9. Diagram of measurement setup.

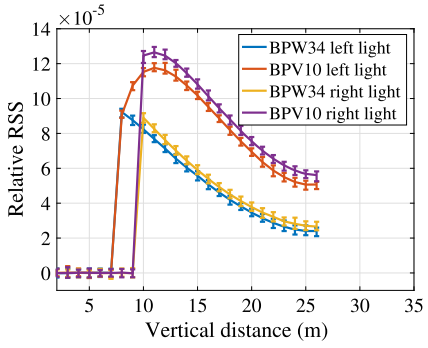

Fig. 10. RSS vs. vertical distance. (For interpretation of the colors in the figure(s), the reader is referred to the web version of this article.)

headlights can be reflected back to its source and hence isolated. Without this feature, the system would have problems tackling the weighted sum of the reflected optical signals from multiple light sources.

7. Experimental results

The experimental results of RSS in terms of different vertical distances between the vehicle and the RPM are presented in Fig. 10. The RSS transits from noise level suddenly to peak level at 6 and 10 meters of vertical distances between the vehicle and the RPM for the left and right headlights, respectively. This is because the ground region that is very close to the headlight is a blind spot due to the manufacture of headlights.

7.1. lane level positioning

In order to evaluate the 2D location accuracy of the vehicle at different vertical distances, we need to first find out the relationship between the incidence angle and the ratio of the RSSs. For the left and right headlights, the ratios of the RSSs are shown in Fig. 11. The results indicate that the ratio of RSSs can be uniquely

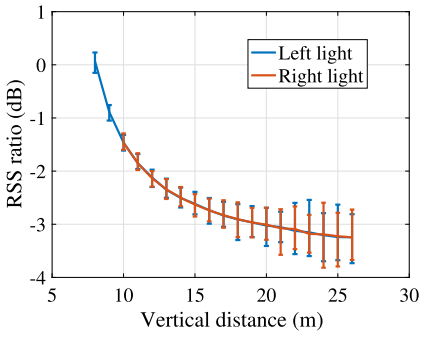

Fig. 11. Ratio vs. vertical distance.

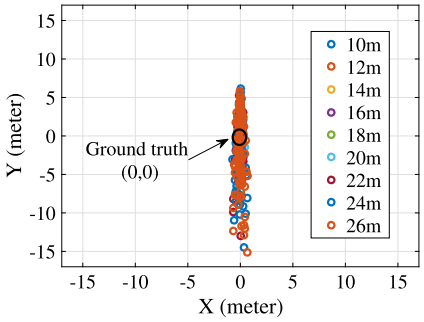

Fig. 12. Candidate 2D locations estimated at different vertical distances.

mapped to the incidence angle. Also as the vertical distance increases, the distinguishability of RPMs (i.e., landmarks) severely degrades. The relationship between the incidence angle and the ratio of RSS is first formulated by polynomial curve fitting based on the average ratio for different incidence angles. Then the values of θ_l and θ_r are estimated by substituting the measurement of RSSs at different vertical distances into the polynomial function generated by curve fitting. Based on the triangulation positioning method elaborated in Sec. 4.2, the 2D, horizontal and vertical location errors for different vertical distances are presented in Figs. 13, 14 and 15, respectively. When the pair of RPMs is close to the vehicle (e.g., vertical distance is less than 14 meters), the 2D location error is at sub-meter level. As the vertical distance increases, the 2D location error increases quickly to several meters and even above 10 meters after the vertical distance exceeds 20 meters. In the next subsection, dead reckoning and Kalman filter are integrated to improve the location accuracy. Nonetheless, Fig. 14 shows that the horizontal location error (i.e., the offset to the central line of a lane) is at sub-meter level for all the vertical distances. The 2D location error is dominant in vertical direction (i.e., traveling direction) as shown in 15. Therefore, the lane in which the vehicle is traveling can still be determined accurately. To evaluate the distribution of the location error, we plot in Fig. 12 the candidate locations calculated by the triangulation positioning method at different vertical distances. It can be observed that the location error mainly occurs at the vertical direction, which indicates that the lane level positioning can be realized based on the existing retroreflective transportation infrastructure.

7.2. in-lane level positioning

In order to further reduce the 2D location error, especially the error occurs at the vertical direction, we apply the advanced positioning solution with ideal dead reckoning (Sec. 5.2) and with Kalman filter (Sec. 5.3) to our experimental measurements. The interval of RPMs is set to 18 meters. The vehicle calculates its 2D location only based on the triangulation positioning method (i.e.,

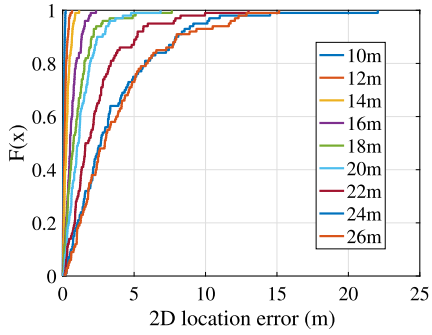

Fig. 13. Empirical CDF of 2D location error for different vertical distances.

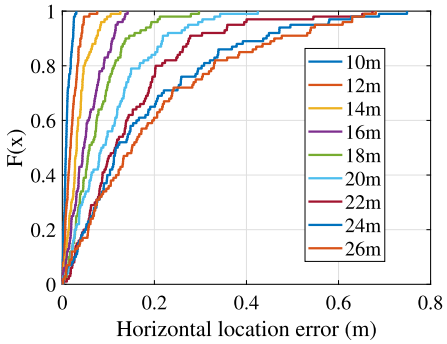

Fig. 14. Empirical CDF of horizontal location error for different vertical distances.

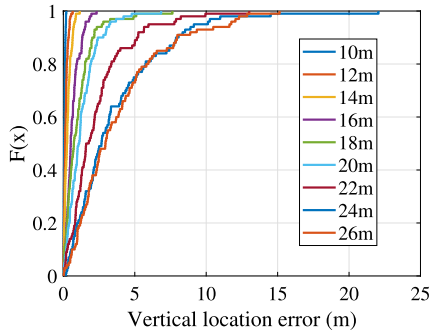

Fig. 15. Empirical CDF of vertical location error for different vertical distances.

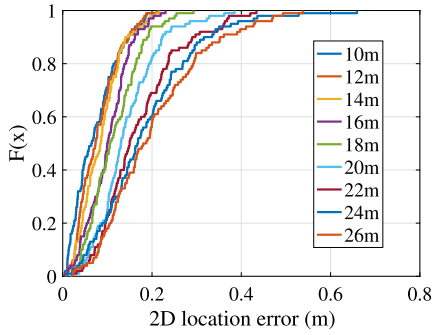

Fig. 16. Empirical CDF of 2D location error with ideal dead reckoning for different vertical distances.

resolving (1), (2) and (3)) when the vertical distance is 10 meters. For the vertical distances from 12 to 26 meters, the traveled distance D accumulated from the location calculated at 10 meters is taken into account (i.e., resolving (1), (2), (3) and (4) or (9)). For instance, denote the location calculated at 10 meters by (x_c, y_c) and the location that the vehicle is trying to figure out when the vertical distance is 26 meters by (x_n, y_n), then we have

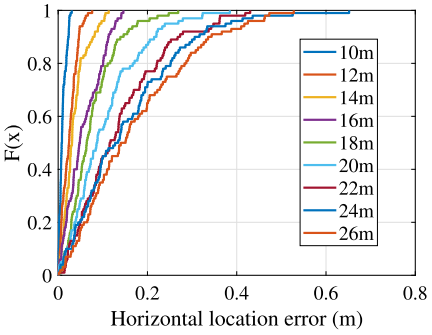

Fig. 17. Empirical CDF of horizontal location error with ideal dead reckoning for different vertical distances.

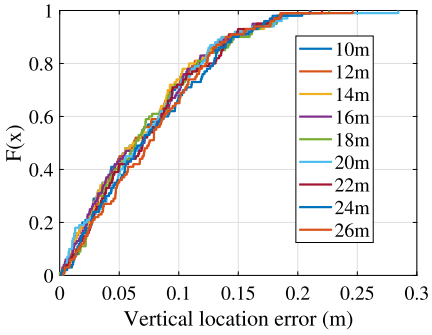

Fig. 18. Empirical CDF of vertical location error with ideal dead reckoning for different vertical distances.

$D = \sqrt{(x_n - x_c)^2 + (y_n - y_c)^2)} = 10 + 18 - 26 = 2$. An example of traveling path diagram is shown in Fig. 22. The vehicle is moving from the starting position (0,0) to the ending position (0,16). At the starting position (0,0), the vehicle senses the AoA from RPMs 1 and 2 and thereby the vertical distance is 10 meters. At position (0,2), the vehicle can only sense the AoA from RPMs 3 and 4 and thereby the vertical distance is 26 meters. Also at position (0,2), the traveled distance $D = 2$.

Based on the advanced positioning method with ideal dead reckoning in Sec. 5.2, the 2D, horizontal and vertical location errors for different vertical distances are presented in Figs. 16, 17 and 18, respectively. By integrating the traveled distance since the last recorded accurate location, the 2D location error during the traveling path is reduced to sub-meter level. The horizontal location error increases as the vertical distance increases while the vertical location error stays at the same level for different vertical distances. The improvement of location accuracy based on dead reckoning mainly acts on the vertical direction. When Kalman filter (Sec. 5.3) is integrated with the advanced positioning method, in (5), B is set to 0.1 second and v_t is Gaussian distributed with mean 20 m/s and variance $\sigma_w^2 = 1$. The 2D, horizontal and vertical location errors for different vertical distances are presented in Figs. 19, 20 and 21, respectively. It is interesting to observe that the 2D location error of Kalman filter is even slightly better than that of ideal dead reckoning. We believe the reason is that the underestimation of D caused by Kalman filter constrains the solution searching process when solving the system equations (1), (2), (3) and (9) such that the horizontal location error is suppressed. The results of location error of the three proposed techniques are summarized in Table 1. In Table 2, we compare our proposed positioning method to GPS, cellular and WiFi in terms of the mean location error. In Fig. 23, Fig. 24 and Fig. 25, considering Fig. 22 as the ground truth, we plot the candidate traveling trajectory calculated by averaging the candidate locations over the 100 measurements with only AoA-based positioning, with ideal dead reckoning and with Kalman filter, respectively. In Fig. 23, the candidate lo-

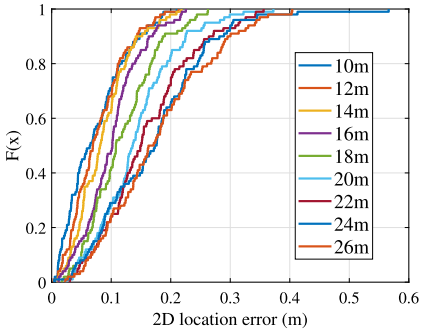

Fig. 19. Empirical CDF of 2D location error with Kalman filter for different vertical distances.

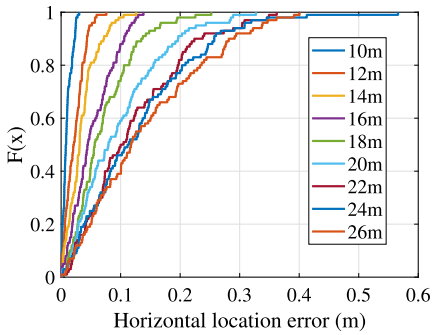

Fig. 20. Empirical CDF of horizontal location error with Kalman filter for different vertical distances.

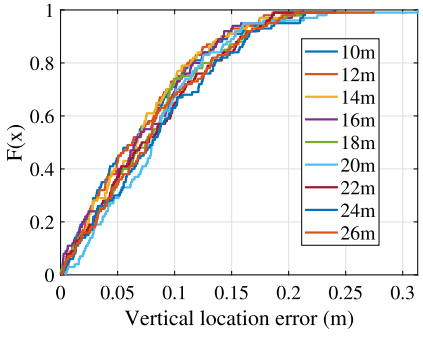

Fig. 21. Empirical CDF of vertical location error with Kalman filter for different vertical distances.

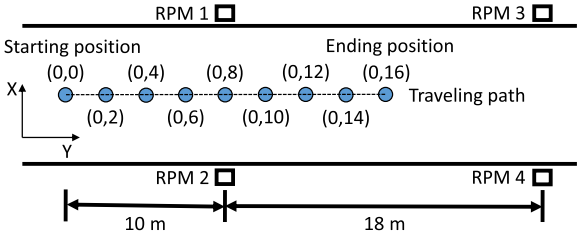

Fig. 22. Traveling path diagram.

cations *loc*2 and *loc*3 are highly deviated from the ground truth while the candidate locations *loc*4 to *loc*9 are getting closer to the ground truth gradually. This is because at *loc*2, the vehicle starts utilizing the AoA from RPMs 3 and 4 to perform the positioning and the vertical distance keeps decreasing as the vehicle moves from *loc*2 to *loc*9. In Fig. 24 and Fig. 25, all the candidate locations are close to the ground truth while the horizontal location error is further reduced when Kalman filter is adopted.

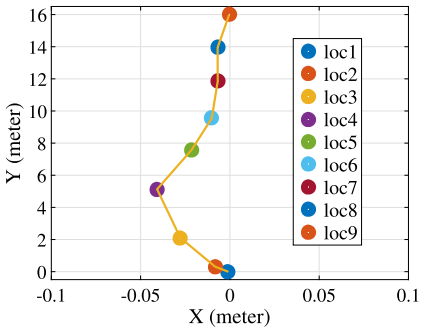

Fig. 23. Candidate traveling path without dead reckoning.

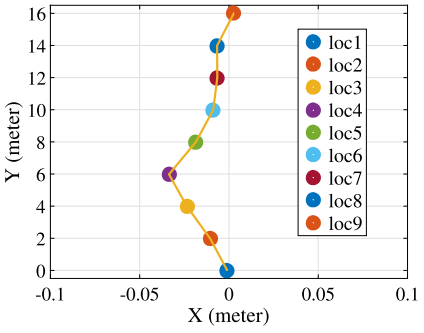

Fig. 24. Candidate traveling path with ideal dead reckoning.

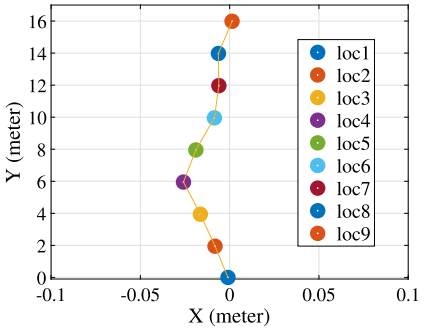

Fig. 25. Candidate traveling path with Kalman filter.

Table 1
Location errors of the proposed positioning techniques. (The 2D location error, horizontal location error and vertical location error listed in the table are the maximum errors in 90 percents of the cases.)

Technique	2D error	Horizontal	Vertical
Only AoA and triangulation	10 m	0.5 m	10 m
With ideal dead reckoning	0.4 m	0.4 m	0.15 m
With Kalman filter	0.3 m	0.3 m	0.15 m

Table 2
Comparison of mean location error of different positioning approaches.

Technique	GPS [24]	Cellular [6]	WiFi [25]	Proposed
Mean error	5–10 m	18 m	3–10 m	0.2 m

8. Discussion

Scalability When we apply the proposed retroreflective VLC system to intelligent vehicular networks, a communication session is generally started by the reader, thus it is the reader's responsibility to ensure that the channel is idle before the session starts. However, due to the directionality of light propagation and the property of retroreflectivity, the reader cannot sense the channel as CSMA in

802.11 networks. Proper multiple access propotol design needs to be explored to tackle the uplink collision (i.e., tag-to-reader) and the downlink collision (i.e., reader-to-tag). To have a comprehensive understanding of the scenarios where the uplink or downlink collisions may take place, the network topology (i.e., the number of involved readers and tags and the connections among them) must be classified for different purposes of the interaction between the readers and the tags. One example is our proposed vehicle positioning system. Since the information piggybacked by the landmarks is small and simple, the landmarks (i.e., RPMs) only need to keep broadcasting the beacon signal including the identification and the coordinates. Passing vehicles interrogate the landmarks by shedding headlights on them and sense the retroreflected optical signal which provides both the location information of the landmarks and the relative angle to the vehicles. Multiple vehicles shedding light on a single landmark will not cause interference among the on-vehicle signal sensing units due to retroreflectivity of the landmark. Another example is that vehicles traveling in different lanes communicate with each other via the RPMs installed between lanes, in this case even though the number of simultaneously active downlinks may be small (typically equal to two), the communication latency resulted from collision avoidance overhead is critical.

Power consumption One potential issue of running the driving circuits of the landmarks could be the power supply. Since there are many such landmarks deployed on the roadways to support the ubiquitous vehicle positioning, it is essential to sufficiently prolong the battery depletion time of the retroreflective devices or even render them completely self-sustaining. In [11], we experimentally evaluate the power consumption of the retroreflective device. Without optimizing the circuit level configuration, the driving circuit and the LCD shutter only cost around 200 μW. It can be expected that the power consumption can be further reduced by optimizing the circuitry design. In [11], we have also theoretically verified that a solar cell with the area of 25 cm^2 is sufficient to operate the driving circuit and the LCD shutter under indoor illumination. For the RPMs exposed under the sunlight, the external solar energy is even more powerful than the indoor lighting. Therefore, it is promising to resolve the power consumption issue of the retroreflective devices by energy harvesting. We will explore experimentally in the future the self-sustaining capability of the retroreflective devices. Since the devices also need to operating during night time, we will investigate the solar charger circuit for small batteries which harvests the excessive energy in the day time and supply the driving circuit during night time.

9. Conclusion

In this paper, we propose a complementary vehicle positioning system by leveraging the on-road safety devices, such as RPMs, as landmarks to support lane-level positioning. Dual-PD receiver placed on the headlights is utilized to sense the AoA information of the LCD-modulated retroreflected optical signals. The modulated optical signals are distinguished from the reflection of on-road objects and from different RPMs as well as to deliver the identification and the location of the RPMs. The AoA and triangulation positioning method is adopted to determine the 2D coordinates of the vehicle. Dead reckoning and Kalman filter are integrated with the proposed vehicle positioning system along the traveling path to further enhance the location accuracy and realize in-lane level positioning. Based on the experimental results, our proposed system achieves sub-meter level location accuracy.

Declaration of competing interest

The authors declare that they have no known competing financial interests or personal relationships that could have appeared to influence the work reported in this paper.

References

[1] B. Hofmann-Wellenhof, H. Lichtenegger, J. Collins, Global Positioning System: Theory and Practice, Springer Science & Business Media, 2012.
[2] Wikipedia, https://en.wikipedia.org/wiki/Global_Positioning_System. (Accessed 7 November 2018).
[3] P. Misra, P. Enge, Global Positioning System: Signals, Measurements and Performance, second edition, Ganga-Jamuna Press, Massachusetts, 2006.
[4] H. Blomenhofer, G. Hein, E.T. Blomenhofer, W. Werner, Development of a real-time DGPS system in the centimeter range, in: IEEE Position Location and Navigation Symposium, 1994, pp. 532–539.
[5] H.S. Cobb, GPS Pseudolites: Theory, Design, and Applications, Stanford University, Stanford, CA, USA, 1997.
[6] C.-H. Chen, C.-A. Lee, C.-C. Lo, Vehicle localization and velocity estimation based on mobile phone sensing, IEEE Access 4 (2016) 803–817.
[7] A. Vidyarthi, H.H. Fan, A navigation solution using HD radio signals, in: Proceedings of the 2015 International Technical Meeting of the Institute of Navigation, January 26–28, 2015.
[8] Velodyne, https://velodynelidar.com/. (Accessed 15 October 2018).
[9] J. Jiang, G. Ananthanarayanan, P. Bodik, S. Sen, I. Stoica, Chameleon: scalable adaptation of video analytics, in: ACM SIGCOMM, 2018, pp. 253–266.
[10] X. Xu, Y. Shen, J. Yang, C. Xu, G. Shen, G. Chen, Y. Ni, PassiveVLC: enabling practical visible light backscatter communication for battery-free iot applications, in: ACM MobiCom, 2017, pp. 180–192.
[11] S. Shao, A. Khreishah, H. Elgala, Pixelated vlc-backscattering for self-charging indoor iot devices, IEEE Photonics Technol. Lett. 29 (2) (2017) 177–180.
[12] US government, https://www.gps.gov/systems/gps/performance/accuracy/. (Accessed 7 November 2018).
[13] A.N. Knaian, A wireless sensor network for smart roadbeds and intelligent transportation systems, Ph.D. dissertation, Massachusetts Institute of Technology, 2000.
[14] S. El-Tawab, S. Olariu, Communication protocols in FRIEND: a cyber-physical system for traffic flow related information aggregation and dissemination, in: 2013 IEEE International Conference on Pervasive Computing and Communications Workshops, PERCOM Workshops, IEEE, 2013, pp. 447–452.
[15] Y.-D. Huang, M. Barkat, Near-field multiple source localization by passive sensor array, IEEE Trans. Antennas Propag. 39 (7) (1991) 968–975.
[16] Y.-S. Kuo, P. Pannuto, K.-J. Hsiao, P. Dutta, Luxapose: indoor positioning with mobile phones and visible light, in: Proceedings of the 20th Annual International Conference on Mobile Computing and Networking, ACM, 2014, pp. 447–458.
[17] C. Zhang, X. Zhang, Pulsar: towards ubiquitous visible light localization, in: ACM MobiCom, 2017, pp. 208–221.
[18] Z. Yang, Z. Wang, J. Zhang, C. Huang, Q. Zhang, Wearables can afford: light-weight indoor positioning with visible light, in: ACM MobiSys, 2015, pp. 317–330.
[19] L. Hu, D. Evans, Localization for mobile sensor networks, in: ACM MobiCom, 2004, pp. 45–57.
[20] A. Grant, J. Bloomfield, et al., Guidelines for the use of raised pavement markers, United States, Federal Highway Administration, Tech. Rep., 1998.
[21] F. Jiménez, J. Naranjo, F. García, J.M. Armingol, Can low-cost road vehicles positioning systems fulfil accuracy specifications of new adas applications? J. Navig. 64 (2) (2011) 251–264.
[22] S. Rezaei, R. Sengupta, Kalman filter-based integration of dgps and vehicle sensors for localization, IEEE Trans. Control Syst. Technol. 15 (6) (2007) 1080–1088.
[23] C. Hu, W. Chen, Y. Chen, D. Liu, et al., Adaptive Kalman filtering for vehicle navigation, J. Glob. Position. Syst. 2 (1) (2003) 42–47.
[24] M. Elazab, A. Noureldin, H.S. Hassanein, Integrated cooperative localization for vehicular networks with partial GPS access in urban canyons, Veh. Commun. 9 (2017) 242–253.
[25] E. Adegoke, J. Zidane, E. Kampert, C.R. Ford, S.A. Birrell, M.D. Higgins, Infrastructure Wi-Fi for connected autonomous vehicle positioning: a review of the state-of-the-art, Veh. Commun. (2019) 100185.